OPEN ACCESS
IOP Publishing
Superconductor Science and Technology
Supercond. Sci. Technol. **35** (2022) 115007 (11pp)
https://doi.org/10.1088/1361-6668/ac95d7

Effect of winding methods: transport AC losses in CORC coils

J Zhao[1], S Y Gao[1], B H Wu[1], X S Yang[1,*], B Shen[2,3,*], W Chen[4] and Y Zhao[1,5,6]

[1] Superconductivity and New Energy R&D Center, Southwest Jiaotong University, Chengdu 610031, People's Republic of China
[2] Electrical Engineering Division, Department of Engineering, University of Cambridge, Cambridge CB3 0FA, United Kingdom
[3] Clare Hall, University of Cambridge, Cambridge CB3 9AL, United Kingdom
[4] School of Intelligent Manufacturing and Electronic Engineering, Wenzhou University of Technology, Wenzhou 325035, People's Republic of China
[5] College of Physics and Energy, Fujian Normal University, Fuzhou 350117, People's Republic of China
[6] Fujian Provincial Collaborative Innovation Center for Advanced High-Field Superconducting Materials and Engineering, Fujian Normal University, Fuzhou 350117, People's Republic of China

E-mail: xsyang@swjtu.edu.cn and bs506@cam.ac.uk

Received 29 July 2022, revised 15 September 2022
Accepted for publication 28 September 2022
Published 7 October 2022

Abstract

AC losses undoubtedly increase the burden on the cooling system and affect the overall performance of high-temperature superconducting (HTS) cables. Therefore, AC losses in HTS cables are important design factors for large-scale HTS equipments. Extensive research has been conducted on straight, densely wound conductors. However, AC losses of bending/circular HTS cable conductors have not been sufficiently studied. In this article, the transport AC losses in a circular HTS conductor coil bended by a conductor on round core (CORC) type cable were investigated using experiments and numerical simulations. The effect of different winding methods was also studied. First, the modeling method of the three-dimensional simulation and the experimental procedures were presented. The simulation results of the straight densely wound conductor (SDWC) and circular densely wound coil (CDWC) were compared with the corresponding experimental results. Finally, the winding method for the CDWC was optimized using both the simulation and experimental approaches. Both the experiments and simulations showed that reducing the tape-to-tape frontal area was able to decrease the transport AC loss, and the results show that the optimum winding angle of the HTS CORC coil was 24.15°. Overall, the modeling and experiments provide useful optimization strategies for designing winding structures of high-performance CORC coils/magnets.

Keywords: HTS conductor, AC loss, CORC coil/magnet, winding method

(Some figures may appear in colour only in the online journal)

* Authors to whom any correspondence should be addressed.

1. Introduction

Second-generation (2G) high-temperature superconducting (HTS) coated conductors have excellent physical properties, such as high critical current density, high upper critical field, strong mechanical and thermal stability [1–3], which lead HTS conductors to be widely used in various high-field devices. These devices must ensure the long-term stable operation of superconductors, where the heat generated by AC losses is an important design factor. The AC loss characteristics of various HTS cables [4–6] have been extensively studied, such as conductor on round core (CORC) [7–12], twisted stacked tape cable [13, 14], Roebel cable (Roebel) [15–17], and quasi-isotropic superconducting cables [18, 19].

In 2007, CORC cables were first proposed by van der Laan while studying the axial strain in the superconducting tape $YBa_2Cu_3O_{7-\delta}$ [3]. The CORC is a conductor wrapped around the cylinder former using HTS tape, which has a high current-carrying density [20], strong mechanical properties [21], and low AC losses [22] because of its special geometric structure. Significant researches on the mechanical and electromagnetic behaviors of straight CORC have been carried out, such as the effect of axial tension on the critical current of a straight CORC [23], quenching behavior of straight CORC detected by Hall sensors [24] and simulation analysis [25], winding mechanics of straight CORC using simulation techniques [26], magnetization loss reduction in straight CORC using laser cutting technology [27], and transport AC losses of straight CORC using the three-dimensional $\boldsymbol{H}$ formulation [28]. The effect of the screening current on the electromagnetic properties of CORC cables is determined using the ***T-A*** formulation [29]. The existing works on AC losses in straight CORC conductors/cables has provided important guidance for pursuing long-distance and high-current HTS cables.

For circular-type CORC, Xiao *et al* [30] experimentally investigated the critical current of CORC cables under cyclic bending-straightening. van der Laan *et al* [31] used an integrated fiber approach to study the quenching behavior of bending CORC. Hu *et al* [32] investigated the stress distribution in bending-type CORC cables using numerical simulations. In 2020, van der Laan *et al* [33] tested a CORC cable based solenoid with currents exceeding 4 kA in a 14 T background field. Jin *et al* [34] tested China Fusion Engineering Test Reactor high-field magnets made from CORC cables. In 2021, Wang *et al* [35] developed and tested the current-carrying capacity of 2.9 T dipole magnets using CORC. In 2022, Zhai *et al* [36], together with Advanced Conductor Technologies, developed Compact Fusion Tokamak Solenoids, and successfully tested them in the presence of large background magnetic fields to verify the maturity and stability of the magnet. For these existing CORC coils/magnets, the basic winding structure is circular. However, the corresponding AC losses have not been systematically studied yet. In this article, the effect of the winding methods of CORC coils on transport AC losses was investigated using experiments and numerical simulations, which can be beneficial for the deep optimizations of various CORC coils in large-scaled high-field magnets, such as the future Tokamak.

2. Numerical simulation

2.1. *T-A formulation*

The ***T-A*** formulation [37–41] assumes the superconducting layer as a thin thickness-free superconducting layer. The current and magnetic fields are calculated by coupling $\boldsymbol{T}$ and $\boldsymbol{A}$. The equation for $\boldsymbol{T}$ was derived from Faraday's law, which was used to calculate the current distribution in the thin layer of the superconductor. The equation for $\boldsymbol{A}$ was derived from Ampere's law and is applied to all domains to calculate the magnetic field profile.

The current vector potential $\boldsymbol{T}$ is defined by the current density $\boldsymbol{J}$:

$$\boldsymbol{J} = \nabla \times \boldsymbol{T}. \tag{1}$$

In the conductor shell, only one component of the current is tangential to the tape surface, whereas the current vector potential $\boldsymbol{T}$ is always perpendicular to the tape surface. $\boldsymbol{T}$ can be written as $T \cdot \boldsymbol{n}$. Therefore, in the conductor surface region, equation (1) can be rewritten as:

$$\begin{bmatrix} J_x \\ J_y \\ J_z \end{bmatrix} = \begin{bmatrix} \frac{\partial (T \cdot n_z)}{\partial y} - \frac{\partial (T \cdot n_y)}{\partial z} \\ \frac{\partial (T \cdot n_x)}{\partial z} - \frac{\partial (T \cdot n_z)}{\partial x} \\ \frac{\partial (T \cdot n_y)}{\partial x} - \frac{\partial (T \cdot n_x)}{\partial y} \end{bmatrix} \tag{2}$$

where n_x, n_y, n_z are the components of vector $\boldsymbol{n}$. The ***E-J*** relationship of the ReBCO conductor is expressed as

$$\boldsymbol{E}(\boldsymbol{J}) = E_0 \left(\frac{|\boldsymbol{J}|}{J_c(\boldsymbol{B})} \right)^n \frac{\boldsymbol{J}}{J_c(\boldsymbol{B})} \tag{3}$$

where $E_0 = 1 \times 10^{-4}\ \mathrm{V\ m^{-1}}$, n is an experimental value of the tape used in this study, and J_c is the critical current density, which is expressed as a function of the field as follows:

$$J_c(\boldsymbol{B}) = J_c(\boldsymbol{B}_{par}, \boldsymbol{B}_{per}) = \frac{J_{c0}}{\left[1 + \sqrt{(k\boldsymbol{B}_{par})^2 + \boldsymbol{B}_{per}^2}/\boldsymbol{B}_c \right]^b} \tag{4}$$

where J_{c0} is the critical current density in the absence of a magnetic field. The parameters $k = 2.2796$, $b = 0.3345$, and $B_c = 115.4$ characterize the anisotropy of the HTS tape.

From equations (2) and (3), and by applying Faraday's law to superconducting shells:

$$\begin{bmatrix} \frac{\partial E_z}{\partial y} - \frac{\partial E_y}{\partial z} \\ \frac{\partial E_x}{\partial z} - \frac{\partial E_z}{\partial x} \\ \frac{\partial E_y}{\partial x} - \frac{\partial E_x}{\partial y} \end{bmatrix} \cdot \boldsymbol{n} + \begin{bmatrix} \frac{\partial B_x}{\partial t} \\ \frac{\partial B_y}{\partial t} \\ \frac{\partial B_z}{\partial t} \end{bmatrix} \cdot \boldsymbol{n} = 0 \tag{5}$$

where B_x, B_y, and B_z are the magnetic flux densities.

The Maxwell–Ampere law is subsequently applied to solve the conventional $\boldsymbol{A}$ equation:

$$\nabla \times \nabla \times \boldsymbol{A} = \mu_0 \boldsymbol{J}. \tag{6}$$

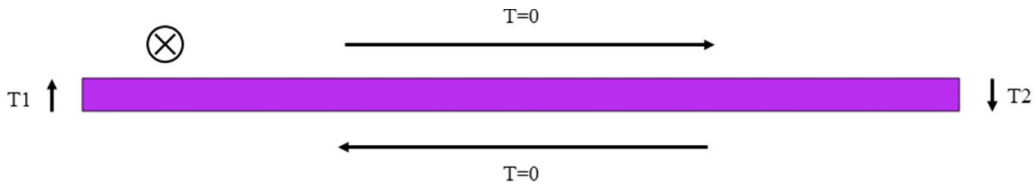

Figure 1. Boundary conditions of a transport current flow in an HTS tape.

If we apply a current at both ends of the conductor coil, we obtain the integral of the current density $\boldsymbol{J}$ over any cross-section of the superconducting tape:

$$I = \iint_s \boldsymbol{J}\mathrm{d}s = \iint_s \nabla \times \boldsymbol{T}dS = \oint_L \boldsymbol{T}\mathrm{d}S \tag{7}$$

where S is the conductor cross-section and L is the boundary edge of the conductor cross-section. As $\boldsymbol{T}$ is perpendicular to the conductor surface, the component parallel to the conductor surface is zero, as shown in figure 1.

Thus:

$$I/t = T_1 - T_2 \tag{8}$$

where T_1 and T_2 are the values of $\boldsymbol{T}$ at the left and right edges, respectively, and t is the thickness of the superconducting layer. The thickness t of the superconducting layer in this article was 1.5 μm. It should note that for the relatively low frequencies used in this article, the effects of multi-layer structures are negligible for calculating transport current losses, and the T-A formulation can well simulate these cases [42–44].

2.2. Numerical modeling of SDWCs

There are many directions of studies can be carried out using the numerical simulation of CORC. This study focuses on the geometric optimization with the analysis on the AC losses and magnetic-field dependence.

2.2.1. Geometric modeling of an SDWC. An SDWC model with the former (outer diameter of 14 mm) and four turns was developed to investigate transport AC losses. Only the superconducting layers of the tape and air domains were included in the model.

One turn of the straight tape is taken from the cylindrical former and unfolded to obtain a parallelogram (figure 2), where r_0 is the outer radius of the former, θ_1 of the dense winding is defined as the angle between the length direction of the tape and the axis of the circular core, and w is the width of the superconducting tape. As the width of the tape is fixed, the angle θ_1 (densely wound onto the round former with radius r_0) is also fixed:

$$\theta_1 = \arccos\left(\frac{w}{2\pi r_0}\right). \tag{9}$$

The pitch P is defined as:

$$P = \frac{2\pi r_0}{\tan(\theta_1)}. \tag{10}$$

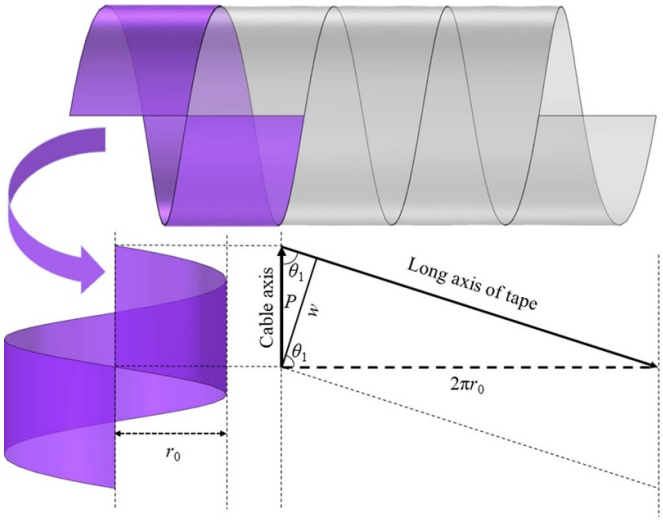

Figure 2. Structure of an SDWC.

2.2.2. Anisotropic magnetic field dependence of SDWCs. The schematic diagram of the magnetic vector decomposition of an SDWC is shown in figure 3. The modulus of perpendicular magnetic field $|\boldsymbol{B}_{\mathrm{per}}|$ and parallel magnetic field $|\boldsymbol{B}_{\mathrm{par}}|$ in the $J_C(\boldsymbol{B})$ equation used for the SDWC can be obtained as follows:

$$|\boldsymbol{B}_{\mathrm{per}}| = B_x\sin(\theta_2) + B_z\cos(\theta_2) \tag{11}$$

$$|\boldsymbol{B}_{\mathrm{par}}| = \sqrt{[B_x\cos(\theta_2) - B_z\sin(\theta_2)]^2 + [B_y]^2} \tag{12}$$

where $\boldsymbol{B}_x$, $\boldsymbol{B}_y$, and $\boldsymbol{B}_z$ are the x-direction, y-direction, and z-direction of magnetic fields, respectively.

2.3. Numerical modeling of CDWC

2.3.1. Geometric modeling of CDWC. This section uses an approximation of the ideal CDWC structure, as the real winding of a CDWC can cause slight deformation of the tape. The CDWC uses the defined conditions of the former direction and tape direction. The CDWC was geometrically analyzed by unfolding the tape on the circular former, as shown in figure 4.

Angle θ in figure 4 is the angle between the length direction of the tape and the direction normal to the circle:

$$\theta = \arcsin\left(\frac{w}{2\pi r_0}\right) \tag{13}$$

where r_0 is the outer radius of the former and w is the width of the superconducting tape. Once the width of the tape and the outer radius of the tape is fixed, the winding angle is fixed.

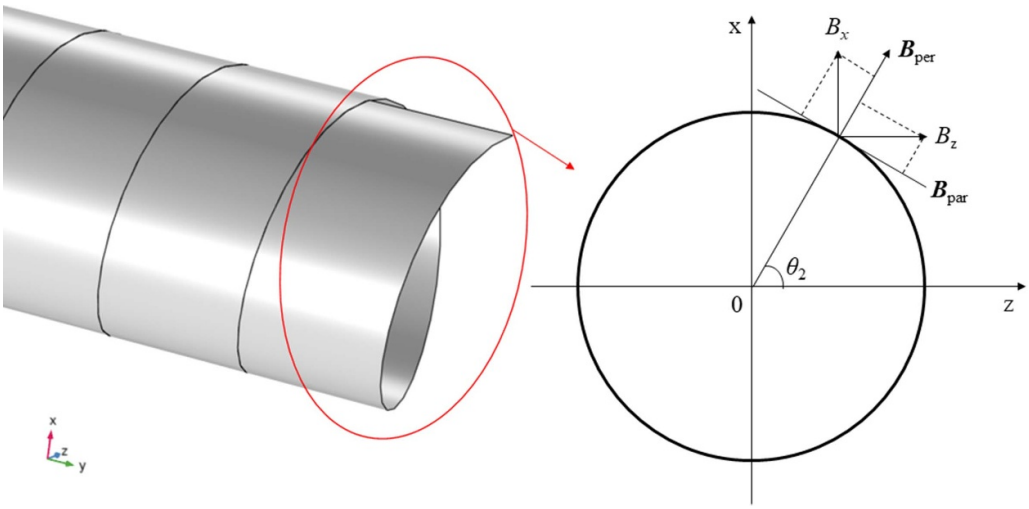

Figure 3. Schematics of the magnetic vector decomposition of an SDWC.

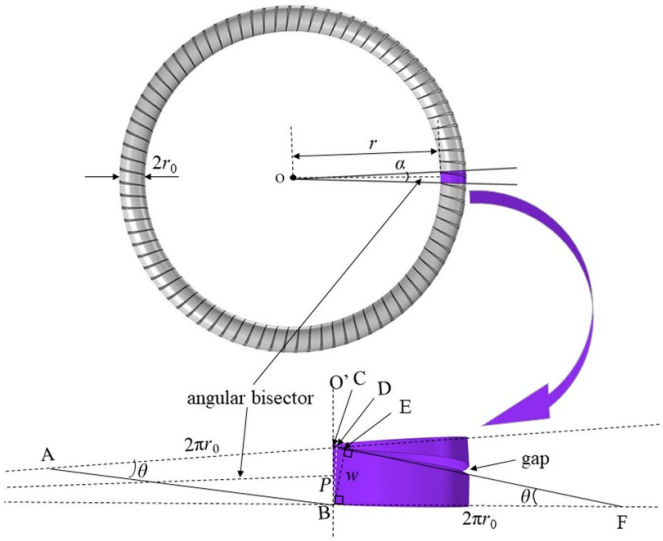

Figure 4. Geometric diagram of a CDWC.

For the convenience of dense winding, the chord length corresponding to the arc length of one turn at radius r of the circle is defined as pitch P:

$$P = 2r\sin\left(\frac{\alpha}{2}\right). \tag{14}$$

Here, α is related to θ, and P is the length of the chord corresponding to angle α. In Rt$\angle$BDF,

$$BD = 2\pi r_0\tan(\theta) \tag{15}$$

$BD \approx P$ when $r + r_0$ is sufficiently large. At this point

$$\alpha = 2\arcsin\left(\frac{r_0}{r}\pi\tan(\theta)\right). \tag{16}$$

The number of turns of the toroidal coil can be expressed as

$$N = \pi/\arcsin\left(\frac{\pi r_0\tan(\theta)}{r}\right). \tag{17}$$

2.3.2. Anisotropic magnetic field dependence of a CDWC. The modulus of perpendicular magnetic field $\boldsymbol{B}_{\text{perp}}$ and parallel magnetic field $\boldsymbol{B}_{\text{para}}$ in the $J_C(\boldsymbol{B})$ equation used in the CDWC are as follows:

$$|\boldsymbol{B}_{\text{perp}}| = B_x\cos(\alpha_1)\cos(\beta) + B_y\sin(\alpha_1)\cos(\beta) + B_z\sin(\beta) \tag{18}$$

$$|\boldsymbol{B}_{\text{para}}| = \sqrt{[B_y\cos(\alpha_1) - B_x\sin(\alpha_1)]^2 + [B_z\cos(\beta) - B_x\cos(\alpha_1)\sin(\beta) - B_y\sin(\alpha_1)\sin(\beta)]^2} \tag{19}$$

where α_1 is the rotation angle along the z-axis. β is the rotation angle of the pipe diameter on the Ω-plane, as schematically shown in figure 5.

The xy-axis in figure 5(b) represents any cross-section along the xy-surface after the center of the circle (note that both the Ω surface and the xy-axis vary with α_1).

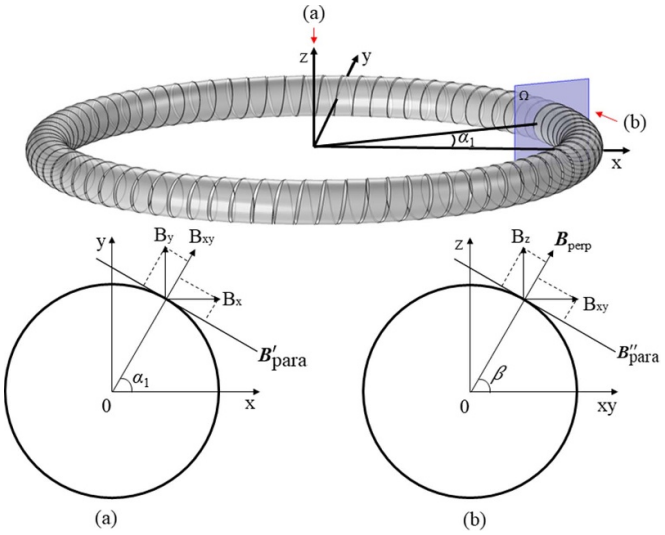

Figure 5. Schematics of the magnetic vector decomposition of a CDWC.

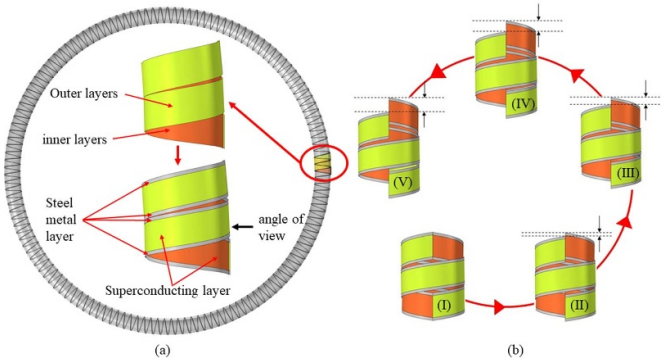

Figure 6. Schematics of the two-layer staggered winding structure for a CORC coil.

2.4. AC losses of the CORC coil

2.4.1. Effect of the interlacing positions on transport AC losses. Multiple layers of tape winding are typically used to increase the current-carrying capacity of the conductors. This section focuses on the effect of the interleaved positions of a densely wound HTS coil with double-layer tape on transport AC losses. The outer diameter of the former was 14 mm, and the diameter of the circle was 280 mm. The current was in the same direction and the layers were interleaved in a reverse manner. Reverse winding of adjacent layers has previously been suggested in the literature [45].

As a result, the outer tape is immobile, while the inner tape rotates counterclockwise around the center with an angle of $\alpha/8$ per rotation. As the circular ring is a symmetric structure, the winding has nine options. However, four options are duplicated, leaving only five final cases (I, II, III, IV, V), as shown in figure 6(b). The AC frequency applied to the model was 79.7 Hz, and the normalized currents were 0.5–0.8 for each of the five cases.

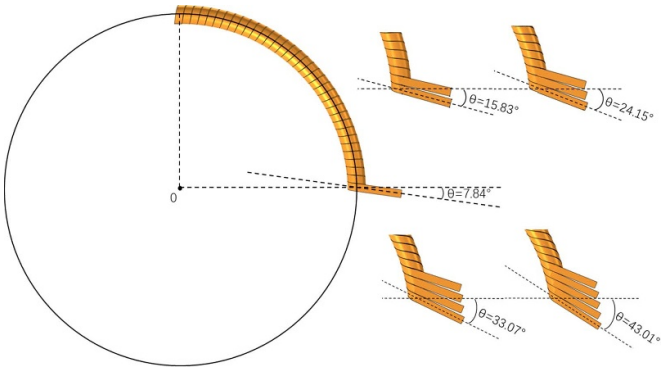

Figure 7. Schematics of CORC coils with different winding methods.

2.4.2. Effect of winding angles on transport AC losses. In this study, the central magnetic field of the CORC coil is an important design index for circular coils, which can be enhanced by changing the winding angle of the tape. The larger current in the circular path is, the larger central magnetic field of the CORC coil will be.

Once the width of the CORC tape and outer diameter of the former were fixed, the winding angle was also fixed to ensure that the tape was densely wound on the former. One tape was densely wound around the former with the first winding angle; subsequently, two side-by-side tapes as one unit were densely wound around the former with the second winding angle. For example, a one-tape dense winding coil had a winding angle of 7.84°, a two-tape dense winding coil had a winding angle of 15.83°, a three-tape dense winding coil had a winding angle of 24.15°, a four-tape dense winding coil had a winding angle of 33.07°, and a five-tape dense winding coil had a winding angle of 43.01°, which were shown in figure 7. The outer diameter of the former was 14 mm, and the diameter of the circle was 280 mm. The AC frequency applied to the model was 79.7 Hz.

3. Experiment

Transport AC losses were measured at 77 K using an electrical measuring platform with a lock-in amplifier, as shown in figure 8.

The AC loss Q_{sc} was calculated by:

$$Q_{sc} = \frac{U.I}{f.L} \tag{20}$$

where U is the RMS value of the loss voltage between the sample leads, I is the RMS value of the AC current collected by the ammeter, f is the frequency of the AC current, and L is the length of the tape between the voltage leads. Since the test sample is a wound coil, the coil generates inductance in the presence of AC current, and this inductance will make the measurement result have a phase difference close to 90°, so the test is compensated by using a compensation coil [46–48].

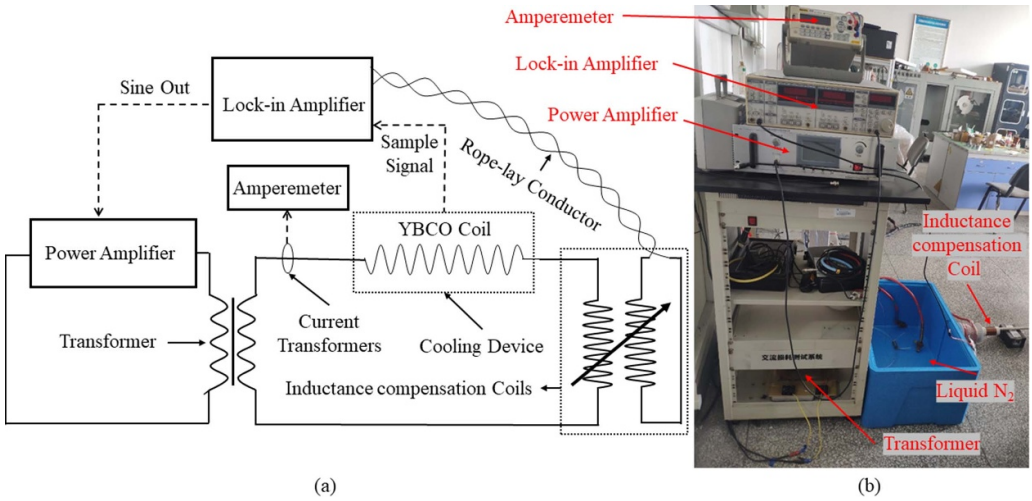

Figure 8. Experiment for AC loss measurement: (a) schematic diagram; (b) photo of the apparatus.

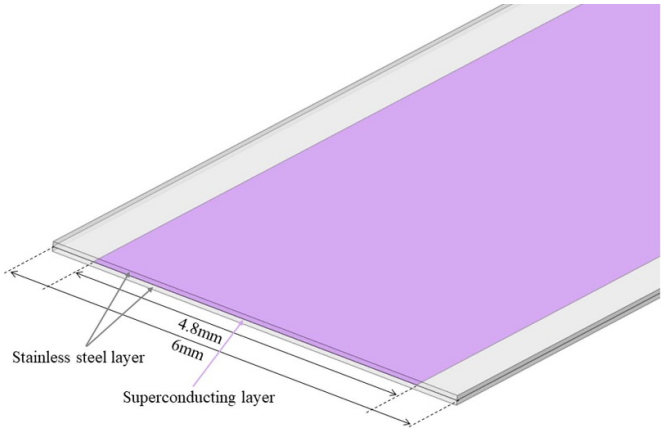

Figure 9. Structure of the 2G HTS tape for experiments.

The superconducting tape used in the experiment was a 2G HTS tape manufactured by Shanghai Superconducting Technology Co., Ltd (product model number: ST-6-L). The overall width of the tape was 6 mm, and the width of the superconducting layer was 4.8 mm (shown in figure 9). The superconducting tapes used for winding the samples were insulated with Kapton tape. Eddy current losses can be induced due to the AC windings on the metal former [11]. However, this experiment only studied the transport AC losses of the tape. Therefore, in this study, a non-metallic polyacrylate material (shown in figure 10(c)) was chosen to build the round core former.

Samples were tested at frequencies of 37.3 Hz, 79.7 Hz, and 113.3 Hz and with different normalized currents between 0.5–0.8. Figures 10(a) and (b) show photos of the SDWC and CDWC samples, respectively.

4. Results and discussions

4.1. SDWC: experiment vs simulation

First, the experimental and simulation results of the SDWC were studied to verify the reliability of the model. The experimental and simulation results were well matched, as shown in figure 11.

The average relative error (experiment and simulation) of the AC losses in the SDWC was 6.54%. The experimental and simulation results were also compared with the Norris (strip) [49], and the results deviated slightly because the Norris (strip) is more applicable to the superconducting sheet structure, which is different from the winding structure on the CORC. Another reason could be: in the CORC structure, the self-field generated by winding the tape can affect the current density distribution inside the tape, because some special field components are perpendicular to the wide surface of the tape, while the anisotropy of the magnetic field is not considered in the Norris equation. It is worth mentioning that normalized critical current is defined as the ratio of the applied current to the critical current.

4.2. CDWC: experiment vs simulation

For the CDWC model, the experimental and simulation results, as well as the Norris (strip), were compared, as shown in figure 12.

The average relative error (experiment and simulation) of the transport AC losses in the CDWC was 6.25%. The experimental data are slightly larger than the simulated data, possibly due to that the model only considered the superconducting layer, but the experimental tape used in this study was a stainless-steel laminated tape. The eddy current losses and coupling losses in other metal layers were not considered in the simulation. Therefore, the experimental curve was larger than the simulation. Another reason could be the inductance of the entire CORC coil, which was not fully compensated by the compensation coil.

In general, for the CDWC, the experiment results well matched the simulation results. Therefore, in this study, the numerical modeling can be fairly useful to predict the performance of practical CORC coils/magnets with good accuracy.

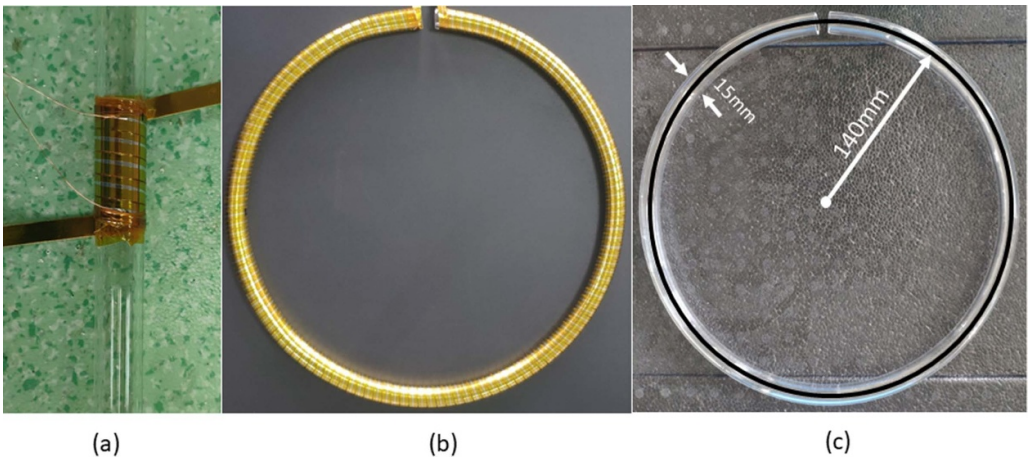

Figure 10. Experimental samples: (a) SDWC; (b) CDWC; (c) CDWC on a polyacrylate former.

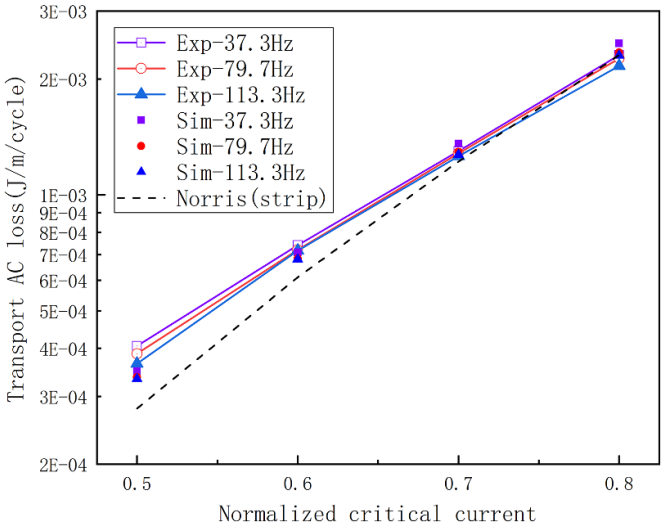

Figure 11. Experiment vs simulation: transport AC losses with different currents, for the SDWC.

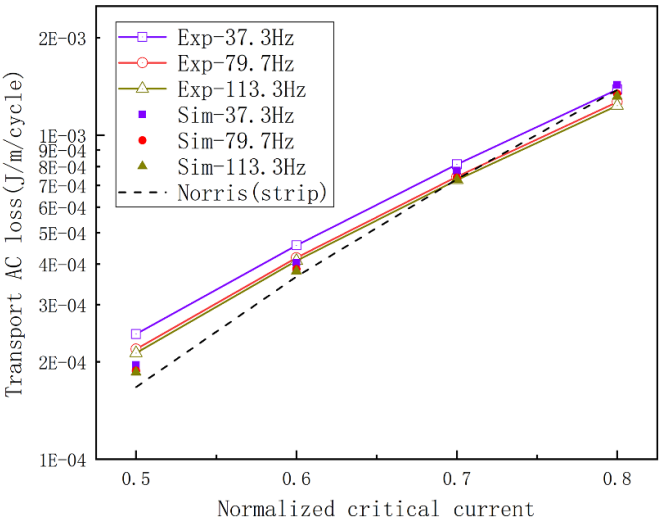

Figure 12. Experiment vs simulation: transport AC losses with different currents, for the CDWC.

4.3. Effect of the winding methods

4.3.1. Effect of the interlacing position. For the staggered winding method (figure 6), both the experiment and simulation results indicated that type-V sample has a smaller AC loss because the front area was smaller than that of type-I sample. In this study, the frontal tape-to-tape area was created in the model, and the corresponding area integral was calculated. The results show that type-V method can reduce approximately 0.1068 mm^2 of the frontal area within a one-turn winding length compared to that of type-I method because the actual width of the superconducting tape was 6 mm, while the superconducting layer width was 4.8 mm. These gaps (figure 6) reduced the frontal area during the circle wrapping process, and also reduced the influence of the perpendicular magnetic field between the superconducting layers. Therefore, it was appropriate to use type-V winding for the adjacent layer of the circular dense-winding coil. In this study, the AC loss of the type-V sample was not much smaller than the AC loss of type-I sample. However, for practical CORC coils, when the coil is large and the tape is used for a long time, there will be a significant difference. In general, reducing the tape-to-tape frontal area reduces magnetization loss caused by the vertical magnetic field. The simulation results are shown in figure 13, and the experimental data are shown in figure 14.

The experimental results of type-V sample and type-I sample showed the same trend as in the simulation. The AC loss of type-V sample at different frequencies was still lower than that of type-I sample.

4.3.2. Analysis of transport AC losses of CDWCs with different winding angles. In figure 15, the simulation results show a linear increase in the central magnetic field of the CORC coil, with an increase in current. As the winding angle increased, the central magnetic field of the CORC coil also increased (figure 15(a)). The central magnetic field increased approximately two-fold when the winding angle of the sample was increased from 7.84° to 15.83°. When the angle was further increased to 24.15°, the central magnetic

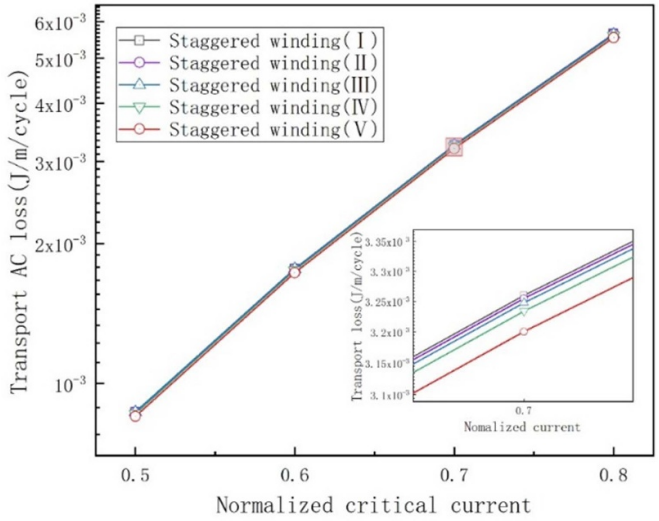

Figure 13. Simulation: transport AC losses at staggered location of two interlaced layers, with different winding method.

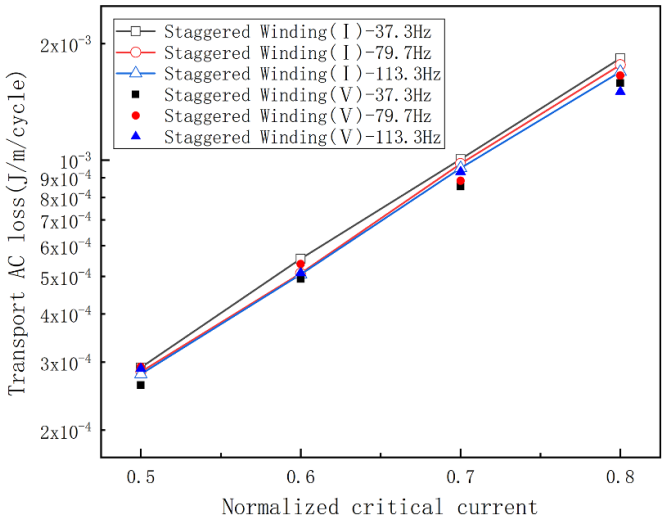

Figure 14. Experiment: transport AC losses with different currents for type-V sample and type-I sample, at different frequencies.

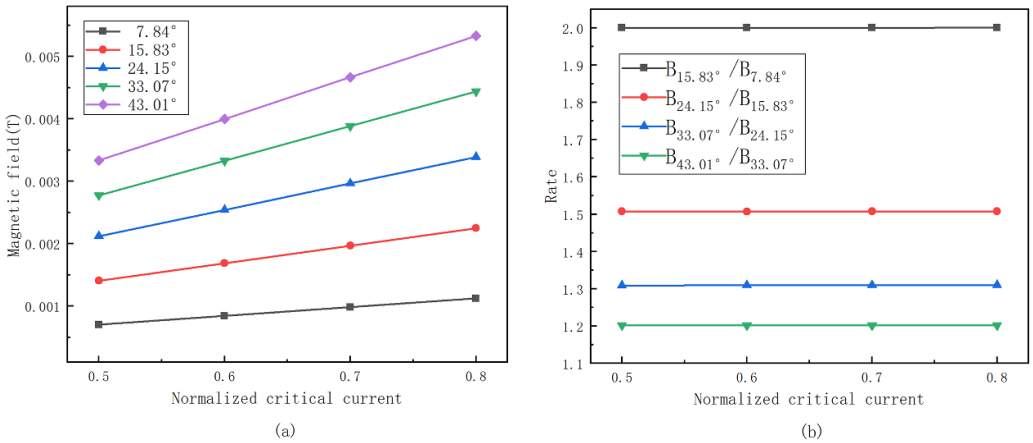

Figure 15. Central magnetic field of the CDWC: (a) central magnetic field of the CORC coil (quarter cycle (peak) of AC) with different currents and with different winding angles; (b) magnetic field ratio with different currents.

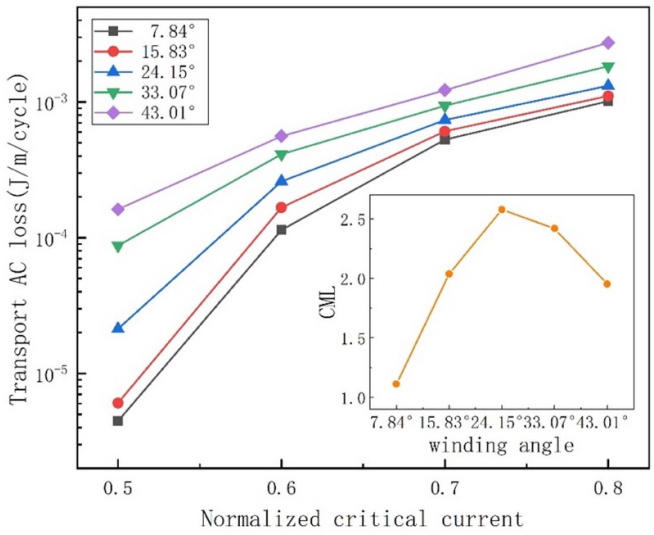

Figure 16. Simulation: transport AC losses with different currents for different winding angles, for the CDWC. Inset: CML (central magnetic field/transport AC loss) at 0.8 I_C with different winding angles.

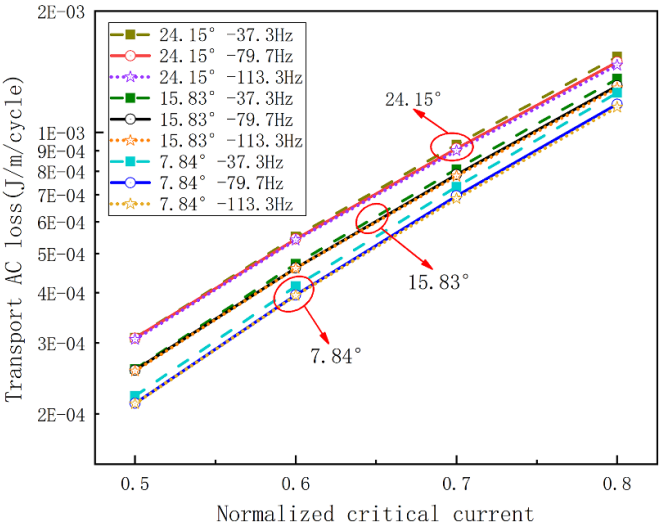

Figure 17. Experiment: transport AC losses with different currents and with different winding angles, for the CDWC.

field was approximately 1.5 times greater than that at the winding angle of 15.83°. The winding angle was gradually increased to 33.07° and 43.01° using a similar method, as shown in figure 15(b). Although the increase rate decayed, the central magnetic field still had an increasing trend.

For the CDWC, increasing winding angle can increase the central magnetic field of the CORC coil. The larger current in the circular path is, the larger the central magnetic field will be. A similar approach can be used for other structures (such as racetrack-shaped and D-shaped) of densely wound CORC coils.

For the transport AC losses, the simulation results (figure 16) show that the AC losses increased with the increasing winding angle and current. The experimental results (figure 17) show the same trend as that of the simulation.

By performing the experiments, transport AC losses at 37.3 Hz, 79.7 Hz, and 113.3 Hz were verified. As shown in figure 17, the transport AC loss at these 3 different frequencies increased with increasing winding angle. In addition, the transport AC losses of the CDWC without a metal former were less dependent on the frequency (figure 17).

For the CDWC, the central magnetic field of the CORC coil and the transport AC loss are contradictory. Therefore, in order to make meaningful analysis, the CML (central magnetic field/transport AC loss) was defined as the evaluation index for the transport AC loss and central magnetic field of the CORC coil. The CML at 0.8 I_C are shown in the inset of figure 16. Evidently, the transport AC loss had a minimum value when the central magnetic field reached a certain value; more specifically, the central magnetic field had a maximum value when the transport AC loss reached a certain value. However, in between, a winding angle of 24.15° leaded to a relatively large central magnetic field but low transport AC losses. Therefore, for the case above, a three-tape dense-winding coil with a winding angle of 24.15° was preferred because of the larger current-carrying capability with relatively low transport AC loss.

5. Conclusion

In this study, the transport AC losses in HTS CORC coils were investigated. Experiments and numerical modeling for the AC losses in the SDWC and CDWC were performed. The accuracy of the ***T*-*A*** formulation model that considers the magnetic field dependence was experimentally verified. For the CDWC, we first investigated two layers of tape-staggered winding coils, and found the transport AC losses of type-V sample were smaller than those of type-I sample, based on experiments and simulations. The CDWC with different winding angles was studied, and the transport AC losses increased with the increasing winding angle and central magnetic field, based on the study of geometric design parameters. The case of three tapes in the CDWC with a winding angle $\theta = 24.15°$ was regarded as the optimum, which had considerably high current-carrying capability but with relatively low transport AC loss. Although the optimal parameters may change with different cases and different configurations of CORC coils, our experimental and modeling methods to study winding approaches, and the evaluation on the AC losses and central magnetic field using CML parameters can be always feasible. To summarize, the modeling and experiments, as well as optimization methods and strategies can be helpful for the future designs of advanced CORC coils/magnets.

Data availability statement

The data that support the findings of this study are available upon reasonable request from the authors.

Acknowledgments

This work was supported by the Sichuan Applied Basic Research Project (Grant No. 2018JY0003), and the National Key R&D Program of China (Grant No. 2017YFE0301402).

ORCID iDs

X S Yang https://orcid.org/0000-0002-8686-9860
B Shen https://orcid.org/0000-0001-8169-6588
Y Zhao https://orcid.org/0000-0002-8774-3629

References

[1] Obradors X and Puig T 2014 Coated conductors for power applications: materials challenges *Supercond. Sci. Technol.* **27** 044003
[2] Samoilenkov S, Molodyk A, Lee S, Petrykin V, Kalitka V, Martynova I, Makarevich A, Markelov A, Moyzykh M and Blednov A 2016 Customised 2G HTS wire for applications *Supercond. Sci. Technol.* **29** 024001
[3] van der Laan D C and Ekin J W 2007 Large intrinsic effect of axial strain on the critical current of high-temperature superconductors for electric power applications *Appl. Phys. Lett.* **90** 052506
[4] Wang Y, Baasansuren S, Xue C and Hasegawa T 2016 development of a quasi-isotropic strand stacked by 2G wires *IEEE Trans. Appl. Supercond.* **26** 4804406
[5] Kang R, Uglietti D and Song Y 2020 Modelling quench of a 50 kA REBCO conductor with soldered-twisted-stacked-tape-cable strands *Cryogenics* **106** 103037
[6] Shi Y, Liu F, Liu H, Tan Y, Zhang X, Jin H, Yu M, Lei L and Guo L 2020 Quasi-round HTS conductor using REBCO tapes for fusion magnet application *IEEE Trans. Appl. Supercond.* **30** 4800104
[7] Šouc J, Vojenčiak M and Gömöry F 2010 Experimentally determined transport and magnetization ac losses of small cable models constructed from YBCO coated conductors *Supercond. Sci. Technol.* **23** 045029
[8] Solovyov M, Šouc J and Gömöry F 2014 AC loss properties of single-layer CORC cables *J. Phys.: Conf. Ser.* **507** 022034
[9] Jiang S, Qian X, Ding H, Chen W, Chen Z, Zou G, Huang P, Guo Y, Jiang D and Kuang G 2020 Optimization research of winding parameters for a single-layer CORC cable *J. Supercond. Nov. Magn.* **34** 417–23
[10] Yagotintsev K, Anvar V A, Gao P, Dhalle M J, Haugan T J, van der Laan D C, Weiss J D, Hossain M S A and Nijhuis A 2020 AC loss and contact resistance in REBCO CORC®, Roebel, and stacked tape cables *Supercond. Sci. Technol.* **33** 085009
[11] Yang J, Li C, Tian M, Liu S, Shen B, Hao L, Ozturk Y and Coombs T 2021 Analysis of AC transport loss in conductor on round core cables *J. Supercond. Nov. Magn.* **35** 57–63
[12] Tian M, Yang J, Shen B, Öztürk Y, Ma J, Li C, Hu J, Wei H, Li J and Coombs T 2021 Analysis on the effect of superconductor layer thickness on the AC loss of conductor on round core (CORC) cables *IEEE Trans. Appl. Supercond.* **31** 5901604
[13] Hong W, Liu H, Liu F, Jin H and Yi S 2022 Improved calculation of magnetic hysteresis loss of stacked superconducting cable under T-A formulation *IEEE Trans. Appl. Supercond.* **32** 5900905
[14] Fu S, Qiu M, Zhu J, Zhang H, Gong J, Zhao X, Yuan W and Guo J 2018 Numerical study on AC loss properties of HTS cable consisting of YBCO coated conductor for HTS power devices *IEEE Trans. Appl. Supercond.* **28** 4802005
[15] Goldacker W, Frank A, Heller R, Schlachter S I, Ringsdorf B, Weiss K P, Schmidt C and Schuller S 2007 ROEBEL assembled coated conductors (RACC): preparation, properties and progress *IEEE Trans. Appl. Supercond.* **17** 3398–401
[16] Song W, Jiang Z, Staines M, Badcock R A and Fang J 2018 Experimental and numerical transport AC losses in a four-strand Roebel cable bifilar stack *Supercond. Sci. Technol.* **31** 115001
[17] Hao L *et al* 2022 Conceptual design and optimisation of HTS Roebel tapes *IEEE Trans. Appl. Supercond.* **32** 5900505
[18] Meng Y, Pi W, Lou X, Ma Y, Wang Y, Kan C and Wang Y 2021 AC losses of quasi-isotropic conductor carrying a DC current in an AC magnetic field *IEEE Trans. Appl. Supercond.* **31** 5900705
[19] Pi W, Sun Z, Zhang Z, Yang Y, Wang R, Ma S and Wang Y 2022 Strain distribution critical and current characteristics of an individual REBCO tape and quasi-isotropic superconducting strand under bending loads by the layerwise theory *IEEE Trans. Appl. Supercond.* **32** 4801307
[20] Weiss J D, van der Laan D C, Hazelton D, Knoll A, Carota G, Abraimov D, Francis A, Small M A, Bradford G and Jaroszynski J 2020 Introduction of the next generation of CORC® wires with engineering current density exceeding 650 A mm^{-2} at 12 T based on SuperPower's ReBCO tapes containing substrates of 25 μm thickness *Supercond. Sci. Technol.* **33** 044001
[21] van der Laan D C, Radcliff K, Anvar V A, Wang K, Nijhuis A and Weiss J D 2021 High-temperature superconducting CORC® wires with record-breaking axial tensile strain tolerance present a breakthrough for high-field magnets *Supercond. Sci. Technol.* **34** 10LT01
[22] Gömöry F, Šouc J, Vojenciak M and Solovyov M 2015 Round conductor with low AC loss made from high-temperature superconducting tapes *IEEE Trans. Appl. Supercond.* **25** 8201004
[23] van der Laan D C, McRae D M and Weiss J D 2019 Effect of monotonic and cyclic axial tensile stress on the performance of superconducting CORC® wires *Supercond. Sci. Technol.* **32** 054004
[24] Weiss J D, Teyber R, Marchevsky M and van der Laan D C 2020 Quench detection using Hall sensors in high-temperature superconducting CORC®-based cable-in-conduit-conductors for fusion applications *Supercond. Sci. Technol.* **33** 105011
[25] Wang Y, Zheng J, Zhu Z, Zhang M and Yuan W 2019 Quench behavior of high-temperature superconductor (RE)$Ba_2Cu_3O_x$ CORC cable *J. Phys. D: Appl. Phys.* **52** 345303
[26] Wang K, Ta W and Gao Y 2018 The winding mechanical behavior of conductor on round core cables *Physica C* **553** 65–71
[27] Li W, Sheng J, Zheng J, Wu Y, Guo C, Li Z and Jin Z 2021 Study on reducing magnetization loss in CORC cables by laser cutting technology *IEEE Trans. Appl. Supercond.* **31** 4802009
[28] Shen B *et al* 2021 Superconducting conductor on round core (CORC) cables: 2D or 3D modeling? *IEEE Trans. Appl. Supercond.* **31** 4803505
[29] Wu Q, Wang Y, Huang Z, Xie Y, He R, Wei J, Lei Z, Qin J and Tan Y 2022 Electromagnetic and mechanical properties of CORC cable due to screening current *IEEE Trans. Appl. Supercond.* **35** 075005
[30] Xiao G Y, zhou C, Qin J G, Jin H, Gao P, Liu H J and Liu F 2021 Experimental study on critical current of bent ReBCO tapes in CORC type cable *Fusion Eng. Des.* **172** 112675

[31] van der Laan D C, Weiss J D, Scurti F and Schwartz J 2020 CORC® wires containing integrated optical fibers for temperature and strain monitoring and voltage wires for reliable quench detection *Supercond. Sci. Technol.* **33** 085010
[32] Hu R, Yuan Y, Chen Y, Li W, Ye H, Sheng J, Zhao Y and Jin Z 2021 Numerical study on mechanical properties of conductors on round core cables *IEEE Trans. Appl. Supercond.* **31** 4801405
[33] van der Laan D C *et al* 2020 A CORC® cable insert solenoid: the first high-temperature superconducting insert magnet tested at currents exceeding 4 kA in 14 T background magnetic field *Supercond. Sci. Technol.* **33** 05LT03
[34] Jin H *et al* 2020 The performance of first CORC cable solenoid insert for development of CFETR high-field magnet *Nucl. Fusion* **60** 096028
[35] Wang X *et al* 2021 Development and performance of a 2.9 Tesla dipole magnet using high-temperature superconducting CORC® wires *Supercond. Sci. Technol.* **34** 015012
[36] Zhai Y, Brown T, Menard J E, van der Laan D C, Weiss J D and Johnson J 2021 HTS cable conductor for compact fusion tokamak solenoids *IEEE Trans. Appl. Supercond.* **32** 4203005
[37] Zhang H, Zhang M and Yuan W 2017 An efficient 3D finite element method model based on the T–A formulation for superconducting coated conductors *Supercond. Sci. Technol.* **30** 024005
[38] Wang Y, Wang Y, Wei D, Guo T and Meng Y 2020 AC losses of a like-corc conductor using accelerated 3D T-A model *Phys. C: Supercond. Appl.* **579** 1353770
[39] Berrospe-Juarez E, Trillaud F, Zermeño V M R and Grilli F 2021 Advanced electromagnetic modeling of large-scale high-temperature superconductor systems based on H and T-A formulations *Supercond. Sci. Technol.* **34** 044002
[40] Shen B *et al* 2021 A simplified model of the field dependence for HTS conductor on round core (CORC) cables *IEEE Trans. Appl. Supercond.* **31** 4803405
[41] Huber F, Song W, Zhang M and Grilli F 2022 The T-A formulation: an efficient approach to model the macroscopic electromagnetic behaviour of HTS coated conductor applications. *Supercond. Sci. Technol.* **35** 043003
[42] Liang F, Venuturumilli S, Zhang H, Zhang M, Kvitkovic J, Pamidi S, Wang Y and Yuan W 2017 A finite element model for simulating second generation high temperature superconducting coils/stacks with large number of turns *J. Appl. Phys.* **122** 043903
[43] Zhang H, Yao M, Kails K, Machura P, Mueller M, Jiang Z, Xin Y and Li Q 2020 Modelling of electromagnetic loss in HTS coated conductors over a wide frequency band *Supercond. Sci. Technol.* **1559** 025004
[44] Bianchetti M, de Bruyn B J H, Krop D C J and Lomonova E A 2020 Simulation of AC losses in racetrack coils wound with striated HTS tapes. *J. Phys. Conf. Ser.* **1559** 012126
[45] Ye H, Li W, Li Z, Li X, Jin Z and Sheng J 2020 Effect of core materials on the electrical properties of superconducting conductor on round core cable *IEEE Trans. Appl. Supercond.* **30** 4800505
[46] Ainslie M, Yuan W, Hong Z, Pei R, Flack T and Coombs T 2011 Modeling and electrical measurement of transport AC loss in HTS-based superconducting coils for electric machines *IEEE Trans. Appl. Supercond.* **21** 3265–8
[47] Wang Y, Guan X and Dai J 2014 Review of AC loss measuring methods for HTS tape and unit *IEEE Trans. Appl. Supercond.* **24** 9002306
[48] Shen B, Li J, Geng J, Fu L, Zhang X, Li C, Zhang H, Dong Q, Ma J and Coombs T 2017 Investigation and comparison of AC losses on stabilizer-free and copper stabilizer HTS tapes *Physica C* **541** 40–44
[49] Norris W T 1970 Calculation of hysteresis losses in hard superconductors carrying ac: isolated conductors and edges of thin sheets *J. Phys. D: Appl. Phys.* **3** 489–507